this plastic was steel as coarse aggregate: Expert

imental and numerical approach

Type

Article

[illegible]

https://knowledge.lancashire.ac.uk/id/eprint/5

8
0
9
0
/
1
0
.
1
2
9
8
9
/
c
a
c
.
2
0
2
6
.
3
7
.
1
.
1
8
1
2
0
2
6
A

Tayeb, Mustafa Maher, Aldahdooh, Majid, Almu

aawali, Saidd, Nazzal, Munir, Tayeh, Bassam

A. Altwair, Nurdeen M. and Hamad, Rami J.

A. (2026) Behavior of sustainable concrete

with plastic waste as coarse aggregate: Exp

experimental and numerical approach. Computers

and Concrete, An International Journal, 37

(1). pp. 181-203. ISSN 1598-8198

,

Mustafa

Maher,

Aldahdooh,

Majid,

Almaawali

i, Said, Nazzal, Munir, Tayeh, Bassam A., A

Itwair, Nurdeen M. and Hamad, Ramiz J. A.

Computers and Concrete, *Vol. 37, No. 1 (2026) 181-203*
https://doi.org/10.12989/cac.2026.37.1.181

Techno-Press

Behavior of sustainable concrete with plastic waste as coarse aggregate: Experimental and numerical approach

Mustafa Maher Al-Tayeb*[1], Majed A. A. Aldahdooh[2], Said Almaawali**[3], Munir Nazzal[4], Bassam A. Tayeh[5,6], Nurdeen M. Altwair[7], Rami J. A. Hamad[8]

[1]*Department of Civil Engineering, Faculty of Engineering, Hasan Kalyoncu University, Şahinbey, Gaziantep, Türkiye*
[2]*Department of Facilities and Construction Project Management, International College of Engineering and Management, affiliated with the University of Lancashire (UK), P.C. 111, Sultanate of Oman*
[3]*Department of Civil and Environmental Engineering, University of Nizwa, Nizwa, Oman*
[4]*Center for Smart, Sustainable & Resilient Infrastructure (CSSRI), Department of Civil & Architectural Engineering & Construction Management, University of Cincinnati, Cincinnati, OH 45221, USA*
[5]*Civil Engineering Department, Faculty of Engineering, Islamic University of Gaza, P.O. Box 108, Gaza Strip, Palestine*
[6]*Department of Civil & Environmental Engineering, University of Waterloo, Waterloo, ON, Canada*
[7]*Civil Engineering Department, Faculty of Engineering, Elmergib University, Khoms, Libya*
[8]*Department of Facilities and Construction Project Management, International College of Engineering and Management, P.C. 111, Muscat, Oman*

(Received August 7, 2025, Revised August 9, 2025, Accepted November 5, 2025)

Abstract. The increasing accumulation of plastic waste (PW) and its low recycling rates pose serious environmental challenges. This study investigates the replacement of coarse aggregate (CA) with polycarbonate PW at levels of 20%, 30%, and 40% in concrete prisms (100×50×400 mm), tested under drop-weight impact loading and validated with finite element method (FEM) simulations. PW incorporation reduced workability (slump from 165 mm to 35 mm) and bulk density (2215 to 1930 kg/m³), alongside compressive strength losses of 25-49% and modulus reductions of 15-34%. However, PW30% demonstrated the highest impact resistance, with a peak Tup load of 14,170 kN at 0.6 ms, bending load of 4152 kN, and inertial load of 5084 kN, confirming its superior energy absorption. Dynamic-to-static ratios also improved with PW, with fracture energy increasing from 3.05 to 10.1. FEM results confirmed these behaviors, particularly for PW30%. Overall, PW30% offers an optimal balance of ductility and toughness, suggesting its suitability for impact-resistant and lightweight applications.

Keywords: finite element modeling; fracture energy; impact loading behavior; plastic waste concrete; sustainable construction materials

1. Introduction

The disposal of plastic waste (PW) is a growing environmental concern due to its increasing production and low recycling rates. In 2022, global PW generation exceeded 400 million tons,

*Corresponding author, Ph.D. Scholar, E-mail: mustafa.altayeb@hku.edu.tr
**Corresponding author, Ph.D., E-mail: salmaawali@unizwa.edu.om

http://www.techno-press.org/cac/5
ISSN: 1598-8198 (Print), 1598-818X (Online)

with projections of further increases by 2050. Despite waste management advancements, only 9% is effectively recycled, while most contributes to landfill overflow and environmental pollution [1]. Microplastic contamination is an emerging dimension of this issue. Sau et al. [2] highlighted the significant occurrence and ecological risks of microplastics in lentic ecosystems, showing how unmanaged plastic waste deteriorates aquatic environments and threatens biodiversity and human health. This further emphasizes the urgency of developing sustainable pathways, such as recycling PW into construction materials. One approach to mitigating this issue is incorporating PW and polymer into concrete as a partial aggregate replacement, aligning with sustainable construction practices and resource conservation strategies [3-10].

Concrete is widely used but suffers from low tensile strength, poor energy absorption, and limited ductility, making it vulnerable to sudden loads in critical elements such as bridge decks, pavements, and industrial floors [11, 12]. Enhancing the impact resistance (IR) and load-bearing capacity of concrete is therefore critical for these applications [12, 13]. Mohammadhosseini et al. [14] demonstrated that incorporating waste metallized PW fibers enhances both the strength and IR of reinforced concrete (RC) composites.

Previous studies have examined the effects of incorporating plastic waste (PW) into concrete, primarily focusing on mechanical properties. Various types of PW, including high-density polyethylene (HDPE), polyethylene terephthalate (PET), and polypropylene, have been used as partial replacements for fine and coarse aggregates and as fiber reinforcement [15-25]. Recent investigations have extended beyond strength aspects to include durability. Sau et al. [26] demonstrated that replacing natural aggregates with recycled PE and PET significantly influenced mechanical and durability properties, including permeability, chloride penetration, abrasion, and impact resistance. Their findings revealed that while higher replacement levels reduce compressive strength, they can improve energy absorption and chloride resistance, emphasizing the dual mechanical-durability effects of plastic aggregate incorporation. In addition, Panda et al. [6] provided a comprehensive review on the use of waste plastics in geopolymer concrete (GPC), highlighting optimal dosages and the influence of plastics on fresh, mechanical, durability, and microstructural properties. Their work shows that PW can also be effectively incorporated in PSGPC systems, further broadening the scope of sustainable construction applications. More recently, Nanda et al. [27] reported that recycled HDPE and PET plastics can serve as coarse aggregate replacements in conventional concrete, with optimal levels of 10% HDPE and 5% PET producing durable and workable mixtures. Their findings highlight the potential of mixed plastic aggregates to promote sustainability while maintaining mechanical performance. Research has largely emphasized compressive strength, with nearly 95% of studies focusing on this parameter, while flexural and splitting tensile strength have received significantly less attention [28, 29]. A summary of literature focus areas versus the current study's objectives is presented in Table 1. Ismail and Al-Hashmi [30] reported that increasing PW content improves workability and reduces unit weight due to its lower density, while Naik et al. [31] found that post-consumer HDPE plastics enhance impact response. Al-Manaseer and Dalal [32]observed that PW particles from vehicle bumpers improve ductility, potentially reducing crack development in structural elements, but also noted that higher PW content reduces compressive and splitting tensile strength. Sau et al. [33] conducted a comprehensive study on green concrete by partially replacing both natural fine and coarse aggregates with recycled polyethylene (RPE) and polyethylene terephthalate (WPET). Their work showed that small replacement levels (up to 10%) can improve flexural strength and maintain splitting tensile strength, while higher levels reduce density and compressive performance. In addition, they integrated artificial neural networks and optimization techniques to

Table 1. Comparative summary of previous studies and the present work

Aspect	Previous studies	Current study
PW type examined	HDPE, PET, PP; mixed post-consumer plastics [16, 17, 18, 30].	Polycarbonate (PC) plastic waste.
Role in concrete	PW used as fine/coarse aggregate replacement [43, 3] and as fibers [34].	Coarse aggregate replacement at 20%, 30%, 40%.
Primary outcome emphasis	Predominantly compressive strength; flexural/splitting tensile less studied [29].	Impact resistance, load-deflection response, and energy absorption (GF).
Impact/ductility evidence	Indications of improved impact response and ductility with PW/HDPE and PW fibers [31, 32, 15].	Impact loading is the central focus with instrumented three-point flexural impact tests (Section 2.4).
Representative replacement levels	Optimization at 30% PW maintained acceptable engineering properties [3].	High PC-PW levels: 20-40% examined systematically (Section 2.2).
Structural/element testing	RC beams for ultimate strength/ductility and beams with openings [18].	Concrete prisms under static and impact flexure with companion cylinders for CS/MOE (Section 2.3-2.4).
Workability & density trends	Increased PW improves workability and reduces unit weight due to lower density [30].	Fresh density/workability tracked across 20-40% PC-PW mixes (Section 2.2).
Strength trade-offs	Higher PW contents reduce compressive and splitting tensile strength [32].	CS/MOE measured alongside impact metrics to quantify trade-offs (Section 2.3-2.4).
Optimization/prediction	RSM/AV optimization and ML predictions [3, 16, 34, 36, 38, 44, 45].	Experimental program with FEM validation; optimization/ML cited for context.
Modeling/validation	Predictive/optimization frameworks discussed; FEM not highlighted in these citations.	Finite element modeling (LUSAS) used to validate L-D behavior and failure patterns (Section 2.5).
Novel contribution (this paper)	Literature largely emphasizes strength metrics; limited direct focus on IR with high PW as coarse aggregate.	First within this set of citations to evaluate high PC-PW (20-40%) for IR with FEM (LUSAS) validation of L-D and GF.

predict and optimize mixture properties, demonstrating the combined potential of experimental and machine learning approaches in PW concrete research.

Kim et al. [34] reported that incorporating recycled PET and polypropylene fibers into RC beams improved ultimate strength by 25% to 32%, depending on fiber content. Mwonga et al. [35] found that PET fiber-reinforced RC beams with openings exhibited ultimate load capacity increases of 4.1% and 5.82% for openings of 0.25h and 0.35h, respectively, while larger openings of 0.45h resulted in a 9.57% strength reduction. These findings indicate that PW fibers influence failure mechanisms, shifting them from shear-dominated to combined shear-flexural failure.

Aldahdooh et al. [3] optimized the use of PW aggregates in conventional concrete using the response surface methodology (RSM), reporting that a 30% PW replacement maintained acceptable engineering properties while offering an alternative to natural aggregates. Building on this, Aldahdooh [36] applied RSM and the Absolute Volume method to develop green concrete incorporating both plastic waste aggregates (PWAs) and sawdust waste (SDW) as partial sand replacements, achieving an optimal balance of compressive strength, workability, and density.

Furthermore, Aldahdooh [37] introduced an integrated framework combining RSM with advanced machine learning and metaheuristic multi-objective optimization to design eco-efficient concrete mixes with multiple waste materials, demonstrating high predictive accuracy (R^2 up to 0.997) and overall desirability of 0.90. These recent contributions highlight the progression from experimental optimization toward hybrid predictive-optimization frameworks for sustainable concrete. In addition, machine learning (ML) has been applied by other researchers to optimize PW concrete mix design and predict mechanical properties. Chao et al. [38] achieved an R^2 of 0.99 for permeability prediction using a BA-ANN model, while Asif et al. [39] reported an R^2 of 0.87 for compressive strength and 0.89 for tensile strength using an MEP model. Han et al. [40] found that RF models yielded a mean absolute percentage error of 2.8% for compressive strength prediction. Mandal et al. [41] further advanced this area by comparing multiple ML techniques, including SVM, ANN, FIS, ANFIS, and GEP, to predict and optimize compressive strength and slump from mixture proportions. Their study identified ANFIS as the most effective model, demonstrating the potential of hybrid ML-optimization frameworks for improving mix design accuracy and cost efficiency.

Previous studies on PW concrete have primarily focused on compressive and flexural strength, with limited attention to impact resistance. This property is critical for pavements, bridge decks, industrial floors, and protective barriers that are frequently exposed to dynamic loads where energy absorption and ductility are required. As summarized in Table 1, most existing research emphasizes mechanical strength, whereas this study addresses impact resistance and validates the findings through FEM analysis in LUSAS. Specifically, the effects of high-volume polycarbonate PW replacement (20%, 30%, and 40%) on impact response, load-displacement behavior, and energy absorption capacity are investigated, highlighting a novel approach at higher substitution levels.

2. Materials and methods

2.1 Materials

This study utilized Ordinary Portland Cement (OPC, ASTM Type I) as the primary binder. The chemical and mineral composition of the cement is presented in Table 2. The oxide composition was determined through X-ray fluorescence (XRF) analysis, and the mineralogical phases (C_3S, C_2S, C_3A, and C_3AF) were subsequently calculated using Bogue's equations in accordance with ASTM C150. These values align with typical OPC characteristics and ensure suitable performance for structural concrete.

Natural coarse aggregate (CA) with a maximum particle size of 10 mm and relative gravity of 2.64 was used, while silica fine aggregate exhibited a bulk density of 1730 kg/m^3 and relative gravity of 2.65, both measured under standard laboratory conditions.

To enhance sustainability, polycarbonate (PC) particles derived from industrial waste were used as plastic waste (PW) aggregates (Fig. 1). The PW aggregates were purchased in a ready-to-use form from a commercial supplier in China (e.g., Shanghai Qishen Plastic Industry Co., Ltd., a leading manufacturer and distributor of PC waste products), and no additional cleaning, crushing, or preparation processes were required. The particle size distribution of CA and PW is presented in Fig. 2. Results show that all PW particles passed through the 5 mm sieve, categorizing them as fine aggregate, whereas CA contained larger fractions, with 100% passing the 14 mm sieve and

Table 2. Cement mineral and oxide compositions

Mineral composition		Oxide composition	
Component	Percentage (%)	Component	Percentage (%)
C_3S	63.12	CaO	64.18
C_2S	9.60	SiO_2	19.96
C_3A	8.19	Al_2O_3	5.18
C_3AF	9.95	Fe_2O_3	3.28
-	-	MgO	0.78
-	-	SO_3	2.39
-	-	Alkalis (Na_2Oeq)	0.92
-	-	Insoluble residue	0.22
-	-	Loss on ignition	2.51

Figure 1. Polycarbonate (PC) plastic waste aggregates used in this study

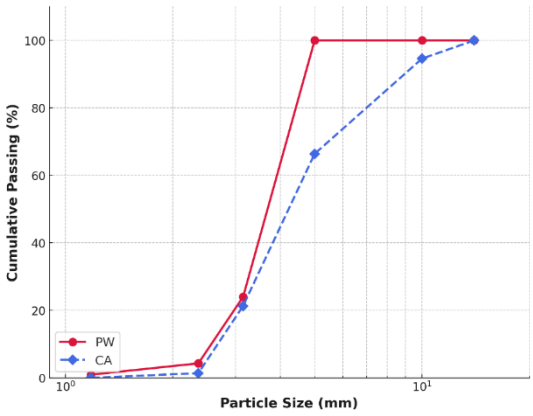

Figure 2. Particle size distribution for the coarse aggregate (CA) and plastic wastes (PW) aggregates

only 1.4% passing the 2.36 mm sieve.

The mechanical and physical properties of PW aggregates are summarized in Table 3. Compared with natural aggregates, PW showed much lower relative gravity (1.22) and unit weight (655 kg/m^3), indicating its lightweight nature. Additionally, the significantly lower Young's

Table 3. Mechanical and physical characteristics of PW aggregates

Characteristics	PW
Color	Black
Relative gravity	1.22
Unit weight (kg/m^3)	655
Young's modulus (MPa)	2610

Table 4. Normal and PW-concrete mix design

Concrete mixtures	Replacement levels [CA-PW]%	Cement (kg/m^3)	CA (kg/m^3)	Fine aggregate (kg/m^3)	Water (kg/m^3)	PW (kg/m^3)
PW0%(Plain)	0.0%	400	970	800	200	0.0
PW20%	20%	400	770	800	200	73
PW30%	30%	400	680	800	200	110
PW40%	40%	400	580	800	200	146

modulus (2610 MPa) highlights the reduced stiffness of PW compared to natural aggregates, which directly influences the mechanical response and ductility of the resulting concrete mixtures.

2.2 Mix proportion and design

Table 4 presents the mix proportions for the control concrete (PW0%) and the PW-modified concretes (PW20%, PW30%, PW40%), illustrating the systematic replacement of coarse aggregate (CA) with polycarbonate plastic waste (PW). The cement (400 kg/m^3), fine aggregate (800 kg/m^3), and water (200 kg/m^3) contents were deliberately kept constant across all mixes to maintain a uniform water-to-cement ratio and ensure meaningful comparability. As the PW content increased from 0 to 146 kg/m^3, the corresponding CA content was reduced from 970 to 580 kg/m^3. This replacement strategy, designed using the absolute volume method, accounts for the lower density and stiffness of PW compared to natural aggregates, factors that directly affect density, workability, and mechanical performance. By varying only the CA-PW ratio while maintaining constant binder, sand, and water, the experimental program effectively isolates the influence of PW incorporation on strength and impact-related behavior. Such an approach is consistent with established practices in waste aggregate research [3], while also highlighting an inherent trade-off: higher PW levels can enhance energy absorption and ductility but may reduce compressive strength due to the inferior mechanical properties of PW. Accordingly, Table 4 not only defines the experimental framework but also provides the basis for evaluating the balance between sustainability benefits and structural performance.

2.3 Sample preparation

In this study, concrete specimens were prepared to evaluate compressive strength (CS), modulus of elasticity (MOE), and flexural behavior under static and impact loads. For CS and MOE testing, three cylindrical specimens per mix were cast, each measuring 200 mm in height and 100 mm in diameter. For flexural testing, three prism specimens per mix were prepared for the

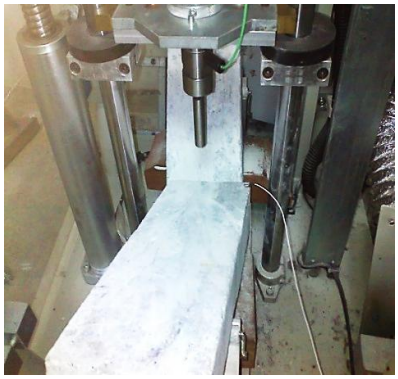

(a) Impact flexural test rig

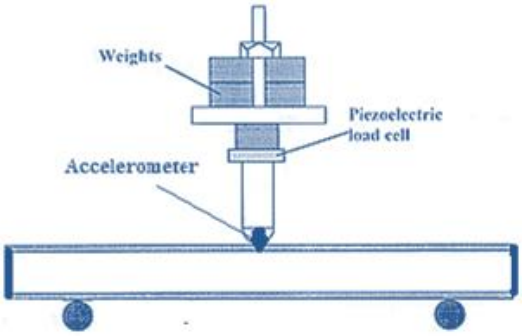

(b) Schematic diagram of the impact flexural test rig

Figure 3. Experimental impact flexural test rig (a) Photographic view of the test rig, (b) Schematic diagram

three-point impact flexural loading test, with dimensions of 50 mm in depth, 100 mm in width, and 400 mm in length, and a loaded span of 300 mm. Additionally, three prisms of identical dimensions were produced for the three-point static flexural loading test, ensuring consistency across test conditions. In accordance with ASTM [47], all specimens were cured in water for 28 days to achieve full hydration and uniform strength development before testing.

2.4 Experimental setup and procedure

In this study, the compressive strength (CS) and static modulus of elasticity (MOE) of the concrete specimens were determined in accordance with ASTM C39 [37] and ASTM C469 [38]. Respectively. Additionally, the three-point static flexural strength was evaluated following the procedures outlined in ASTM C78/C78M [39]. The impact response of the specimens was examined using an instrumented falling weight impact machine, as illustrated in Fig. 3. The setup in this study featured a 2 kg drop hammer, which could be released from heights ranging from 0.5 m to 2 m. For this experiment, the hammer was dropped from a height of 0.5 m to generate controlled impact forces ASTM C469 [38]. A piezoelectric load cell (Kistler 933-A, France) with a 100 kN capacity was positioned slightly above the impactor tup to continuously record the impact force history during testing [48-53]. In this study, the specimens were supported by two steel cylinders (10 mm Ø), placed on adjustable right-angled supports, ensuring consistent boundary conditions [48]. To capture specimen accelerations during impact, a Dytran 3224A2 accelerometer (USA) was mounted at the mid-span of the beam. This accelerometer, used in this study, had a sensitivity of 2 mV/g and could measure accelerations up to ±2500 g. It was securely attached to the top surface of the beam, directly above the impact point, to accurately record acceleration changes [48]. A PC-based data acquisition system was employed in this study to collect signals from both the load cell and accelerometer at intervals of 0.2 μs, ensuring high-resolution recording of the impact event.

The bending load (P_b) at the mid-span of the beam is given by [54-57],

$$P_b = P_t - P_i \tag{1}$$

where P_t is the tup load, and P_i (Eq. (2)) is the inertial load which is uniform along the beam, for linear distribution of accelerations.

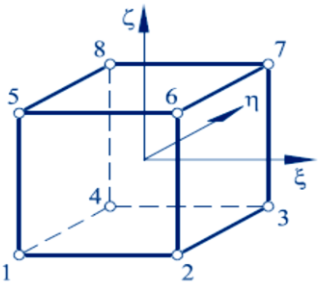

Figure 4. The 8-node hexahedron and the natural coordinates ξ, η, ζ

Table 5. The shape functions for 8-node hexahedron

$N_1^{(e)} = \frac{1}{8}(1-\xi)(1-\eta)(1-\zeta)$ $N_2^{(e)} = \frac{1}{8}(1+\xi)(1-\eta)(1-\mu)$ $N_3^{(e)} = \frac{1}{8}(1+\xi)(1+\eta)(1-\zeta)$
$N_4^{(e)} = \frac{1}{8}(1-\xi)(1+\eta)(1-\mu)$ $N_5^{(e)} = \frac{1}{8}(1-\xi)(1-\eta)(1+\zeta)$ $N_6^{(e)} = \frac{1}{8}(1+\xi)(1-\eta)(1+\mu)$
$N_7^{(e)} = \frac{1}{8}(1+\xi)(1+\eta)(1+\zeta)$ $N_8^{(e)} = \frac{1}{8}(1-\xi)(1+\eta)(1+\zeta)$

$$P_i = \rho A a[L/3 + (8/3) \times (ov^3/L^2)] \quad (2)$$

where ρ: mass density of concrete; A: area of cross-section of the beam; a: acceleration at the center; L: span of the test beam; and ov: length of the overhang. The displacement history $d(t)$ at the load-point is given by [54-57],

$$d(t) = \int_0^t \int_0^t a(t)\, dt \quad (3)$$

where $a(t)$ is the acceleration as function of time.

2.5 Finite element development

In order to simulate the behavior of plastic concrete beams subjected to the impact load, LUSAS was used. The concrete beam was represented by eight corners of hexahedron elements (Fig. 4) using standard shape functions as represented by Eq. (6) [58]. The corresponding shape functions for the eight nodes of the hexahedron are summarized in Table 5.

$$N_i^{(e)}(\xi, \eta, \zeta) = \frac{1}{8}(1+\xi_i\xi)(1+\eta_i\eta)(1+\zeta_i\zeta) \quad (4)$$

The deformation was calculated by using the following expression,

$$\{u\} = \sum_{i=1}^{np}[N_i]\{u_i\} \quad (5)$$

where [42], the deformation vector at any location over the element; u_i: the deformation vector at the specified node of the element; $[N_i]$: the nodal shape function matrix of size (3×3); np: the total number of the nodes in the element.

The boundary conditions (Fig. 5) were set as: The tup load curve obtained from experiment was used to define the load at the location P_t (x=200 mm, y=50 mm, z=50 mm), and the beam was supported (uniformly distributed along z-direction) from bottom at locations, x=50 mm (support 1) and x=350 mm (support 2). Visco-Plastic material was used to model plastic concrete structures.

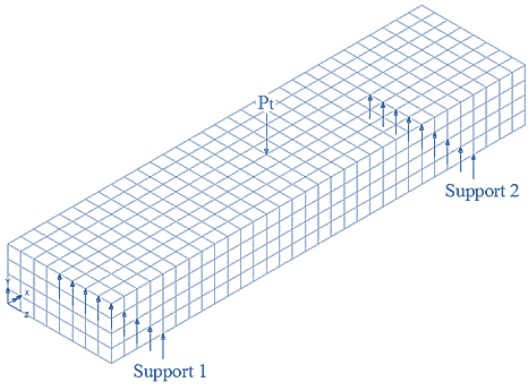

Figure 5. Finite element model for the beam

To choose the appropriate mesh size, a number of trials were made and found that, after 1024 elements there was no improvement in accuracy; hence this mesh size was selected and the simulation took about 30 minutes in a computer with dual-Core Processor i7-7500U 2.7Ghz, 8GB DDR4 Memory, 1TB Hard Drive, USB 3.0.

The nonlinear dynamic equilibrium equation [59, 60] is given by,

$$[M]\{a\} + [C]\{v\} + [K]\{d\} = \{f_e\} \tag{6}$$

where M is the mass matrix which is defined as,

$$[M] = \sum_{e=1}^{n} [N]^{(e)T} [\rho]^e [N]^e dv \tag{7}$$

where N is the element shape function array and ρ is the density matrix. C is the Rayleigh damping matrix expressed by,

$$[C] = a_R[M] + b_R[K] \tag{8}$$

where K is the structure stiffness matrix defined by,

$$[K] = \sum_{e=1}^{n} \int_v [B]^{(e)T} [D]^{(e)} [B]^{(e)} dv \tag{9}$$

where B is the strain displacement matrix and D is material modulus matrix; a_R (Eq. (10)) and b_R (Eq. (11)) are the Rayleigh damping coefficient of mass and stiffness respectively.

$$a_R = \frac{2\varpi_f \varpi_s (\psi_s \varpi_f - \psi_f \varpi_s)}{(\varpi_f^2 - \varpi_s^2)} \tag{10}$$

$$b_R = \frac{2(\psi_f \varpi_f - \psi_s \varpi_s)}{(\varpi_f^2 - \varpi_s^2)} \tag{11}$$

where ψ_f and ψ_s are the damping ratio of the structure for first circular frequency (ϖ_f) and second circular frequency (ϖ_s) respectively [53, 59]. The damping ratio for first circular and second circular frequencies is assumed as 5% [60]. Explicit (central difference) nonlinear dynamic scheme was used to determine the acceleration and thus the velocity and displacement increments for each time step. Explicit scheme was used for problems which require small time steps such as shock response from explosive or impact loading [59].

Table 6. Workability and bulk density of concrete mixtures

Concrete mixture	Slump (mm)	Bulk density (kg/m^3)
PW0% (Plain)	165	2215
PW20%	85	1970
PW30%	55	1950
PW40%	35	1930

In this study, the visco-plastic formulation was chosen because it can represent pressure-sensitive plasticity in concrete and reproduce both tensile cracking and compressive crushing under high loading rates. Tensile failure was captured through a fracture-energy-based softening law, while compressive failure was governed by pressure-dependent plasticity. Interfacial debonding of plastic waste particles from the matrix was represented using a traction-separation approach defined by peak traction and fracture energy. Strain-rate effects were incorporated phenomenologically by scaling static strengths with dynamic amplification factors observed in the experimental impact tests. These assumptions are consistent with the physical behaviour observed in the laboratory and with modelling approaches commonly adopted for concrete beams under impact.

3. Results and discussion

3.1 Experimental results

3.1.2 Effect of plastic waste on workability and bulk density

Table 6 presents the slump values and bulk density for various concrete mixtures, showing a declining trend as the PW content increases. This suggests that the workability and bulk density of concrete mixes are significantly affected by the incorporation of PW. These results are also in agreement with those in Table 4, which suggests that the use of PW results in changes in the properties of fresh and hardened concrete.

The plain concrete mix (PW0%) recorded the highest slump value of 165 mm, while the PW40% mix had the lowest slump value of 35 mm. This indicates that workability decreased with the increase in PW content. This decline is primarily attributed to the differences in particle size distribution between PW and CA, as shown in Table 3. Unlike CA, which contains larger particles with a well-graded distribution, PW consists mostly of smaller particles (100% passing the 5 mm sieve). The lack of larger PW particles results in higher surface area exposure, increasing friction between particles and reducing the fluidity of the mix, thereby making it less workable [16]. Additionally, as shown in Table 3, PW has a lower relative gravity (1.22) and unit weight (655 kg/m^3) compared to CA, further contributing to its poor dispersion within the mix and reduced slump values [16]. At the microstructural level, the hydrophobic nature and irregular surface texture of PW hinder proper bonding with the cement paste, weakening the interfacial transition zone (ITZ) and increasing porosity, which further explains the loss in workability [49, 61-63].

Similarly, the bulk density of concrete decreased with increase in the PW content. To this end, the bulk density dropped from 2215 kg/m^3 for PW0% to 1930 kg/m^3 for PW40%. This confirms that PW-modified concrete is significantly lighter than conventional concrete. This reduction is

Table 7. Mechanical properties of concrete mixtures

Concrete mixture	Average CS (MPa)	Standard deviation - CS (MPa)	Average MOE (GPa)	Standard deviation - MOE (MPa)
PW0% (Plain)	43	0.8	29.25	0.9
PW20%	34	1.0	24.14	0.9
PW30%	28	1.1	23.16	1.0
PW40%	22	1.0	20.84	1.1

Note: CS refers to the compressive strength; MOE refers to the modulus of elasticity.

due to the lower density of PW compared to CA, as evident in Table 3, where PW has a significantly lower unit weight and Young's modulus (2610 MPa) compared to conventional aggregates [16]. In addition, weak ITZ bonding and the presence of entrapped voids around PW particles reduce packing efficiency and contribute to the lower mass per unit volume. The decrease in bulk density suggests that PW-modified concrete has a lower mass per unit volume, which could be advantageous in applications where lightweight concrete is required [54-57].

In summary, the incorporation of PW adversely impacts workability and bulk density, making concrete less fluid and more lightweight. The smaller particle size of PW, lower unit weight, and poor interfacial bonding leading to microstructural porosity contribute to the observed reductions [16]. While reduced workability may present challenges in placement and compaction, the lower bulk density offers benefits in lightweight concrete applications, such as non-load-bearing structures, insulation layers, and floating structures [54-57].

3.1.2 Impact of plastic waste on compressive strength and modulus of elasticity

Table 7 presents the results of mechanical properties of concrete mixes tested in this study. It is noted that the incorporation of PW as a partial replacement for CA significantly reduces the compressive strength and modulus of elasticity of the considered of concrete mix. To this end, the compressive strength of plain concrete was 43 MPa, but it decreased by 25%, 36%, and 49% for PW20%, PW30%, and PW40%, respectively. This reduction can be attributed to changes in bulk density and workability, as highlighted in Table 6, and aligns with previous research by Choi et al. [16]. This reduction is consistent with previous studies, which attribute the decline to the lower compressive strength of PW compared to natural aggregates [16]. As shown in Table 3, PW has a significantly lower unit weight (655 kg/m^3) and Young's modulus (2610 MPa) than natural aggregates, weakening the overall concrete matrix. Additionally, Table 3 highlights the difference in particle size distribution between PW and CA, where PW particles are significantly finer, with 100% passing the 5 mm sieve. The smaller particle size increases the total surface area, requiring more cement paste to coat the particles, leading to weaker bonding and lower structural integrity. The weaker interfacial bond between PW particles and cement paste further contributes to early crack initiation and reduced overall strength.

The results in Table 7 also indicates that the MOE decreased by 15%, 23%, and 34% as PW content increased, which is in agreement with results reported by Choi et al. [16]. This reduction indicates that PW-modified concrete is more deformable, making it more flexible but less stiff than conventional concrete. The slump values in Table 6 show a decline from 165 mm (plain) to 35 mm (PW40%), indicating that PW disrupts mix cohesion, creating a less compact and more porous structure. As shown in Table 4, replacing CA with PW reduces the total aggregate volume,

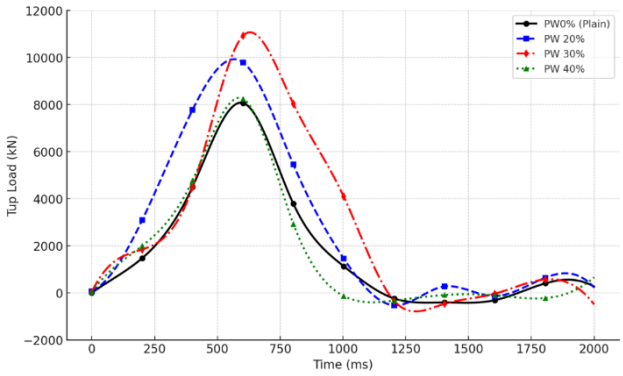

Figure 6. Tup load history for concrete with varying PW substitutions under impact loading

leading to a looser mix with reduced internal friction. The resulting lower density and weaker interfacial bond strength may have contributed to the lower stiffness and strength observed in Table 7.

The reduction in CS and MOE is primarily due to the low stiffness and strength of PW compared to natural aggregates. Additionally, the poor bonding between PW and the cement paste, coupled with the deformability of PW particles, promotes microcrack formation around PW inclusions [16]. This behavior is similar to the effects of air voids in conventional concrete, where weak points in the matrix reduce the material's ability to sustain compressive loads. The lower relative gravity of PW (1.22, Table 3) further contributes to reduced density and strength [16].

The decrease in bulk density suggests that PW-modified concrete has a lower mass per unit volume, which could be advantageous in lightweight concrete applications such as non-load-bearing structures and insulating elements [54-57]. However, while PW improves energy absorption and flexibility, optimizing its interfacial bonding with cement paste is essential to balance strength, stiffness, and ductility.

3.2 Impact performance of PW-reinforced concrete

Fig. 6 presents the tup load history for different PW percentages (PW0%, PW20%, PW30%, and PW40%), illustrating a sharp increase in impact load (I.L), peaking around 600-800 ms, followed by a rapid decline. The results indicate that PW30% exhibits the highest tup load, exceeding 10,000 kN, suggesting enhanced impact resistance (I.R) compared to other mixes. PW20% follows closely, while PW40% and PW0% (plain concrete) demonstrate lower peak loads, implying that excessive PW substitution may reduce impact resistance. The observed negative loads after 1000 ms, particularly for PW30% and PW40%, could be attributed to inertial load (P_i) effects and material rebound. The sustained higher loads for PW30% and PW20% indicate improved flexural resistance, whereas PW40% exhibits an earlier decline, suggesting increased brittleness. Overall, the findings suggest that PW30% is the optimal mix for enhancing impact resistance, while excessive PW substitution (PW40%) may compromise load-bearing capacity due to reduced fracture energy (G_F).

Fig. 7 illustrates the variation of tup load (I.L), bending load (M), and inertial load (P_i) over time for PW0% (Plain), PW 20%, PW 30%, and PW 40% concrete, demonstrating the influence of PW replacement levels on impact resistance (I.R). The results indicate that I.L, M, and P_i increase

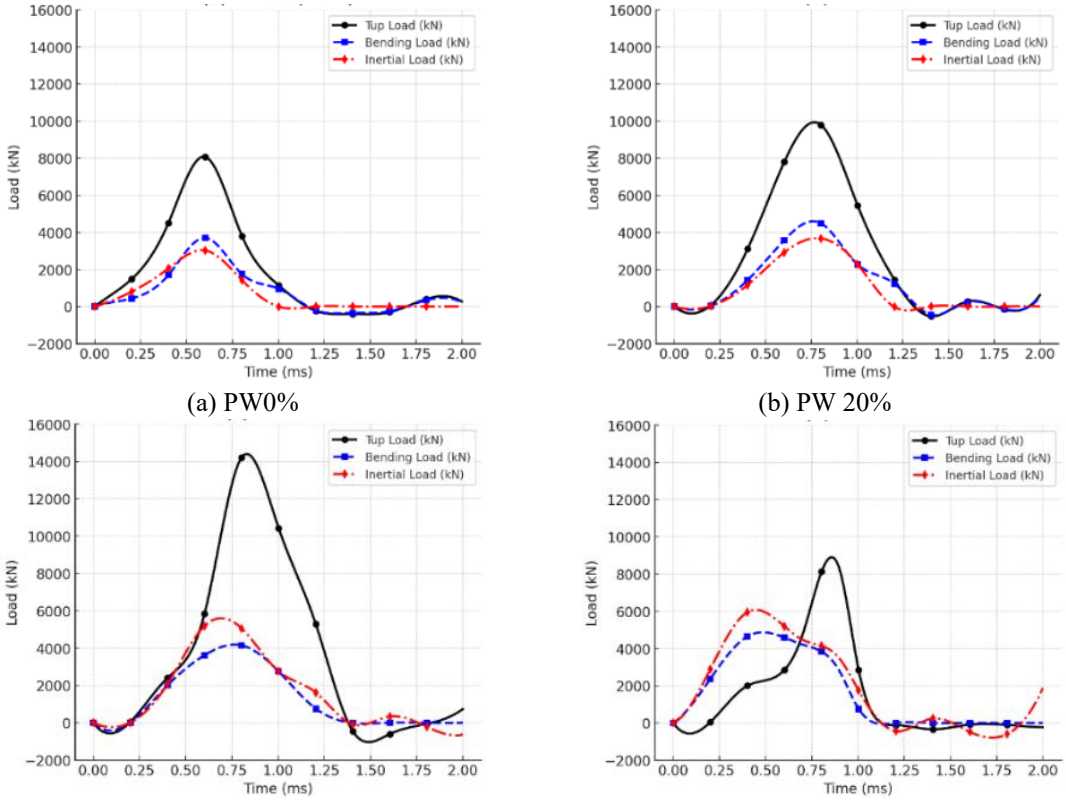

(a) PW0% (b) PW 20%

(c) PW 30% (d) PW 40%

Figure 7. Tup load, bending load, and inertial load over time for different PW percentages

with PW incorporation up to 30%, reaching their highest values in Fig. 7(c) PW 30% before declining in Fig. 7(d) PW 40%. The highest I.L is observed in Fig. 7(c) at 14,170 kN (0.6 ms), followed by Fig. 7(b) at 9810 kN (0.8 ms), Fig. 7(d) at 8255 kN (0.9 ms), and Fig. 7(a) at 8075 kN (0.6 ms). Similarly, M and P_i exhibit higher values for PW 20% and PW 30%, confirming that moderate PW content enhances impact performance, while excessive PW substitution leads to a reduction in structural integrity. These findings align with Asokan et al. [63], who reported that PW enhances ductility and impact energy absorption, contributing to higher I.R at moderate replacement levels.

The observed improvement in M and P_i for PW 20% and PW 30% aligns with Suaris and Shah [65], who stated that materials with lower static bending strengths experience a proportionally higher increase in M under dynamic impact conditions. This explains why M reaches 4501 kN in Fig. 7(b) and 4152 kN in Fig. 7(c), compared to 3701 kN in Fig. 7(a) PW0%. Additionally, Fu et al. [64] demonstrated that fracture behavior in high-strain-rate loading is affected by material ductility and energy dissipation capacity, supporting the increased P_i in Figs. 7(b) and (c), which peak at 3674 kN and 5084 kN, respectively, before gradually declining. However, in Fig. 7(d) PW 40%, M drops to 2784 kN, confirming that excessive PW content reduces the composite's ability to distribute bending stress effectively, leading to earlier failure under impact conditions.

After the peak I.L, a noticeable decline in M and P_i occurs, but the rate and pattern vary across

Table 8. Experimental impact and static bending test results comparison

Concrete type	Impact results		Static results		Ratio: dynamic/static	
	Peak bending load (N)	G_F (Nm)	Peak bending load (N)	G_F (Nm)	Peak binding load (N)	G_F (Nm)
Normal	8080	1.43	4110	0.48	1.98	3.05
PW20%	12910	2.42	3054	0.45	4.24	5.48
PW30%	13710	3.62	2836	0.40	4.84	9.25
PW40%	9270	3.25	2585	0.33	3.59	10.1

the mixes. In Fig. 7(a) PW0% (Plain), P_i reaches zero after 1.0 ms, indicating limited inertial resistance. Conversely, in Fig. 7(b) PW 20% and Fig. 7(c) PW 30%, P_i remains significant until 1.2 ms, demonstrating improved inertia effects. However, in Fig. 7(c) PW 30%, P_i turns negative (-79.00 kN) after 1.2 ms, which suggests post-impact oscillations, a behavior previously reported by Fu et al. [64], who identified inertial instability as a key factor in impact fracture progression. In Fig. 7(d) PW 40%, P_i declines sharply (-431.3 kN at 1.2 ms), and M drops to zero, confirming that excessive PW inclusion weakens the structure, leading to reduced bending performance and early loss of I.R. The negative M values observed after 1.4 ms in Figs. 7(a) and (b) further support the presence of rebound effects, which are common in high-strain-rate impacts, as highlighted by Suaris and Shah [65].

PW30% outperforms PW40% because it attains a practical balance between stiffness and ductility within the composite. At 30% replacement the natural aggregate skeleton remains largely continuous, allowing effective stress transfer through the matrix, while the lightweight polycarbonate particles introduce localized flexibility that improves energy absorption and crack bridging. The physical properties of the PW used (low unit weight=655 kg/m^3 and low Young's modulus=2610 MPa, Table 3) make it effective as an energy-dissipating inclusion but also mechanically weak compared with natural aggregate. At 30% the number and size of weak PW inclusions are sufficient to improve impact toughness (see GF and dynamic/static ratios in Table 8) without breaking the aggregate load path. At 40% the fraction of low-stiffness PW becomes large enough that particle-to-particle spacing and packing are altered, porosity and weak ITZ regions increase, and the continuous natural-aggregate load-bearing network is disrupted Asokan et al. [63]. This promotes earlier microcrack initiation and faster loss of bending capacity under impact, explaining the observed drop in tup, M, and P_i for PW40%. In short, PW30% lies near an optimum threshold where beneficial ductility effects outweigh loss of stiffness, while PW40% exceeds that threshold and becomes detrimental to impact peak capacity.

Figs. 8(a) and 7(b) illustrate the experimental tup load (kN) vs. deflection (m) response for normal concrete (PW0%) and PW-reinforced concrete with 20%, 30%, and 40% PW under impact loading (I.L). The corresponding fracture energy (GF) values are summarized in Table 8, which also compares dynamic and static bending test results. Consistent with previous studies [54-57], dynamic GF exceeds static GF, confirming that PW modification enhances energy absorption under impact conditions.

The normal concrete (PW0%) exhibits a peak load of 8080 N with a GF of 1.43 Nm, while PW20% and PW30% significantly improve GF, reaching 2.42 Nm (+69%) and 3.62 Nm (+153%), respectively. PW40% achieves 3.25 Nm (+127%), but its lower energy absorption compared to PW30% suggests increased brittleness at higher PW content. This trend is evident in Fig. 8(a),

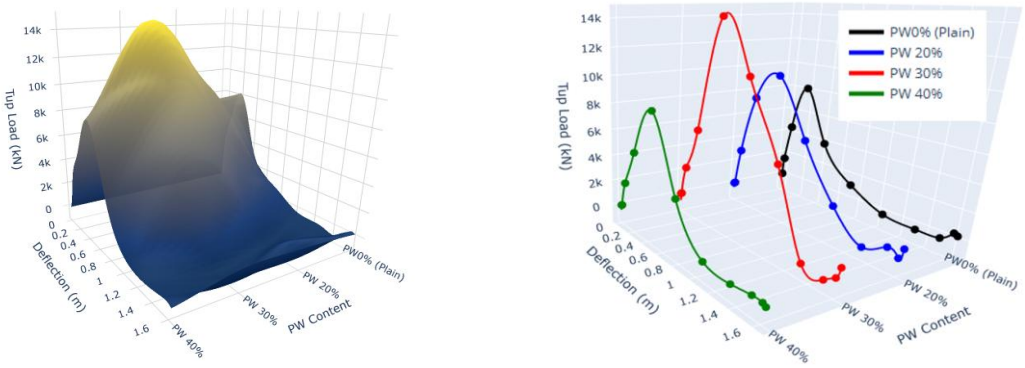

(a) Surface plot (b) Response curves

Figure 8. 3D impact load-experimental deflection response of PW-reinforced concrete

where PW30% maintains the highest peak load (~13710 N) before gradually softening, demonstrating enhanced energy absorption before failure. In contrast, PW40% exhibits a steeper post-peak decline, indicating reduced ductility and potential premature failure, aligning with its higher dynamic/static GF ratio (10.1) compared to 9.25 for PW30%.

Table 8 further supports these findings, showing that PW30% achieves the highest peak impact load (13710 N), followed by PW20% (12910 N) and PW40% (9270 N), with normal concrete at 8080 N. The dynamic/static GF ratio for PW30% is 9.25, emphasizing its superior energy absorption and impact resistance, which is 4.84 times greater than normal concrete. These results confirm that PW30% provides the optimal balance between strength and ductility, while PW40% shows a brittle response despite its higher G_F.

Overall, PW significantly enhances impact resistance, with PW30% demonstrating the most effective balance of peak load capacity and energy absorption. PW40%, despite its higher G_F, exhibits brittle behavior, suggesting a limit beyond which PW addition may reduce ductility. These findings highlight the potential of PW-reinforced concrete for impact-resistant applications and optimizing structural performance.

3.2.1 Comparison of static and dynamic test results

A key observation is that the dynamic-to-static peak bending load ratio increases with PW content, rising from 1.98 for normal concrete to 3.59 for PW40%. Similarly, the dynamic-to-static GF ratio increases from 3.05 for normal concrete to 10.1 for PW40%, confirming the ability of PW to enhance energy absorption under impact loading. However, as PW content increases, the static peak bending load decreases, which is expected since replacing CA with PW reduces interfacial bond strength and makes the matrix more susceptible to static stresses.

At the microstructural level, this is explained by the crack deflection and bridging effects of PW. During impact, the softer and more deformable PW inclusions absorb and dissipate energy through localized deformation, forcing cracks to deviate and propagate around the particles instead of passing directly through [16]. This mechanism enhances fracture energy under dynamic loading. In contrast, under static conditions, weak ITZ regions and higher porosity dominate, allowing cracks to link across voids more easily and thereby reducing static capacity.

Despite the reduction in static capacity, PW enhances impact resistance through flexibility, deformability, and crack-bridging capacity. For example, the dynamic-to-static GF ratio increased

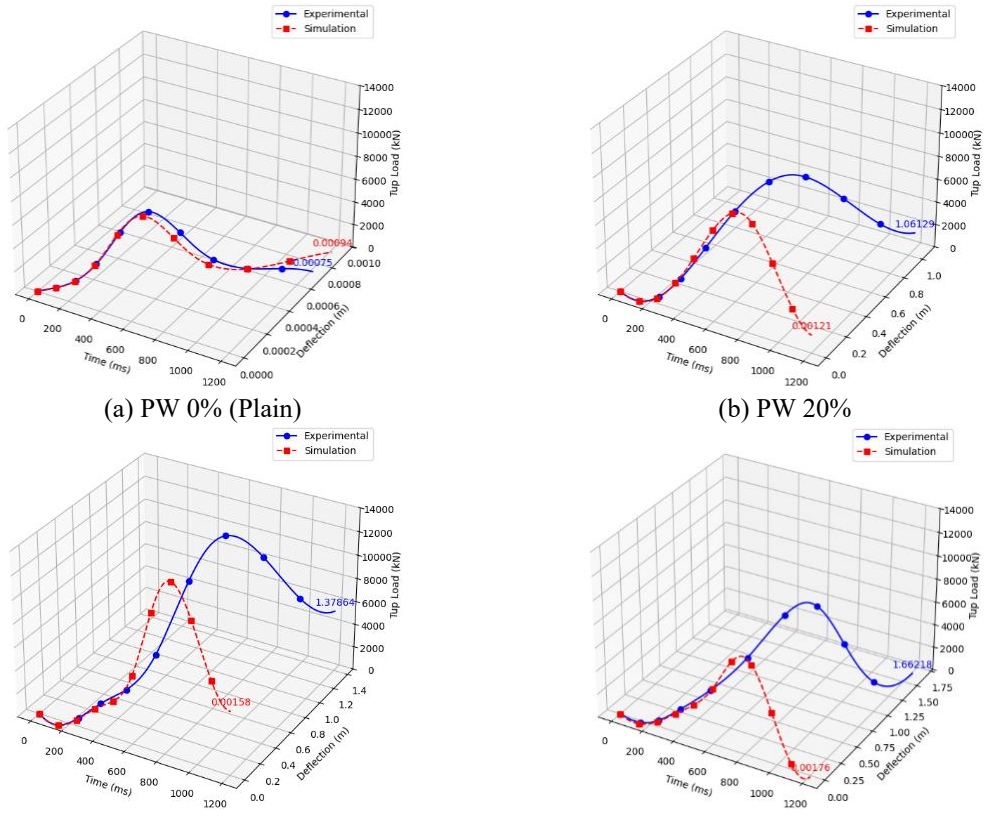

(a) PW 0% (Plain) (b) PW 20%

(c) PW 30% (d) PW 40%

Figure 9. 3D response curves of tup load vs. time vs. deflection (Experimental and simulation) for different PW percentages

from 3.05 for normal concrete to 5.48 for PW20%, 9.25 for PW30%, and 10.1 for PW40% (Table 8). Similarly, the dynamic-to-static bending load ratio rose from 1.98 for normal concrete to 4.24 for PW20%, 4.84 for PW30%, and 3.59 for PW40%. These results demonstrate that while PW30% achieved the best overall balance, higher PW content can still improve energy absorption but at the cost of reduced stiffness.

The combined outcome of increased impact resistance and reduced compressive strength defines clear application limits. The 36% reduction in compressive strength for PW30% (Table 7) restricts its use in primary axial-load members such as columns and heavily loaded beams. However, the marked improvement in fracture energy and dynamic-to-static response suggests that PW30% is particularly well suited for components where toughness and energy absorption are critical, such as protective barriers, crash-resistant panels, industrial flooring, and pavement Asokan et al. [63].Therefore, PW-modified concretes should be functionally targeted: adopt PW30% in secondary or impact-prone elements where resilience is required, but avoid or strengthen PW mixes for use in load-bearing members. Practical next steps include improving interfacial bonding and packing efficiency (for example, through surface treatment or optimized grading) and re-evaluating detailing for structural members where localized toughness is more important than peak compressive strength.

Table 9. Experimental vs FEM predicted results for PW-reinforced concrete

Mix ID	Peak Tup Load (kN)-Exp.	Peak Tup Load (kN)-FEM	Error (%)	Deflection at Peak (mm)-Exp.	Deflection-FEM	Error (%)
PW0%	8075	7924	%1.9	0.00079	0.00093	15
PW20%	9810	9980	%1.7	0.00082	0.00121	32
PW30%	14171	13850	%2.2	0.00097	0.00158	39
PW40%	8682	8746	%0.8	0.00117	0.00176	34

3.2.2 Comparison of the experimental and simulation results

The impact response of plastic waste (PW)-reinforced concrete samples was analyzed by comparing experimental and numerical results across different PW percentages. In Fig. 9(a), the PW 0% (Plain) sample exhibited a peak tup load of 8075 kN at 0.6 ms, followed by a decrease, indicating impact energy dissipation. The experimental deflection increased to 0.00075 m at 1.2 ms, while the simulation underpredicted it, with a maximum of 0.00094 m. The growing divergence suggests the numerical model may not fully capture plastic deformation or strain-rate effects, leading to an underestimation of compliance.

For PW 20%, shown in Fig. 9(b), the peak tup load increased to 9810 kN at 0.8 ms, demonstrating improved impact resistance. However, the experimental deflection was significantly higher, reaching 1.06 m at 1.2 ms, while the simulation predicted only 0.00121 m. A similar trend is observed in PW 30% (Fig. 9(c)), which recorded the highest peak tup load (14,200 kN at 0.8 ms), indicating superior impact resistance. Despite this, experimental deflections were significantly greater than numerical predictions, with 1.38 m vs. 0.00158 m at 1.2 ms, highlighting the model's limitations in predicting large deformations.

For PW40% (Fig. 9(d)), the peak tup load dropped to 8255 kN at 0.8 ms, with experimental deflection reaching 1.66 m, the highest among all mixes. This indicates reduced stiffness and excessive deformation at higher PW content. The FEM underestimated these deflections, highlighting the need for better modeling of softening, strain-rate effects, and failure mechanisms. While moderate PW improved impact resistance, excessive replacement promoted instability and early failure. From a microstructural perspective, this behavior reflects the competing effects of ductile crack bridging by PW and premature ITZ debonding. In PW30%, microcracks are blunted and redirected by well-distributed PW particles, leading to higher fracture energy and a more gradual failure process. At PW40%, however, the dense presence of weak ITZ regions and entrapped voids accelerates localized crack coalescence, explaining the sharp loss of stiffness and the high deflections observed experimentally. The FEM model, which simplifies softening and does not fully capture ITZ porosity and microcrack evolution, underestimates these deformation effects, although it successfully replicates global fracture paths.

The results are further supported by Table 8, which compares experimental impact and static bending test results. The PW 30% sample, which exhibited the highest impact resistance in Fig. 9(c), also recorded the highest peak bending load (13,710 N) and fracture energy (3.62 Nm) under impact testing. However, under static conditions, its peak bending load decreased to 2836 N, resulting in a dynamic-to-static load ratio of 4.84. This suggests that PW 30% benefits the most from strain-rate effects, offering superior impact resistance but undergoing significant deformation under sustained loading.

As seen in Table 9, although deflection magnitudes are underestimated in the simulation, the

consistency in fracture initiation, crack paths, and stress concentration zones indicates that the model effectively captures the global failure behavior of PW 30% concrete under impact. The deflection mismatch likely arises from simplified treatment of softening and rate effects in the current visco-plastic model. Future refinements could include more detailed calibration of fracture energy values, an improved description of tensile softening behaviour, and incorporating rate-dependent parameters across a wider range of strain rates. Such improvements would help reduce the deflection discrepancy while preserving the good agreement observed in fracture initiation and crack distribution.

4. Conclusions

This study evaluated the impact of replacing 20%, 30%, and 40% of coarse aggregate (CA) with plastic waste (PW) on the load-deflection behavior and fracture energy (GF) of concrete prisms under impact loading, compared with static loading and validated through finite element method (FEM) simulations. The following conclusions are drawn:

- The incorporation of PW reduced slump from 165 mm (PW0%) to 35 mm (PW40%) and decreased bulk density from 2215 kg/m^3 to 1930 kg/m^3. This reduction confirms the potential of PW concrete as a lightweight material, though with lower workability.
- Compressive strength (CS) decreased by 25%, 36%, and 49% for PW20%, PW30%, and PW40%, respectively, compared with PW0% (43 MPa). Similarly, modulus of elasticity (MOE) dropped from 29.25 GPa at PW0% to 20.84 GPa at PW40%, indicating reduced stiffness and increased deformability with higher PW replacement.
- PW30% exhibited the highest impact resistance, recording a peak tup load of 14,170 kN at 0.6 ms, bending load (M) of 4152 kN, and inertial load (P_i) of 5084 kN. This demonstrates superior energy absorption and toughness. PW20% showed improved resistance compared with PW0% (9810 kN at 0.8 ms), while PW40% recorded lower peak loads (8255 kN at 0.8 ms) and excessive deformation, confirming that excessive PW weakens structural integrity.
- PW30% achieved the highest fracture energy (GF=3.62 Nm) under impact loading, with a peak bending load ratio of 4.84 between dynamic and static conditions. Dynamic-to-static ratios increased with PW content, reaching 10.1 for GF at PW40%. These results confirm that PW enhances strain-rate sensitivity and toughness but compromises static compressive performance.
- FEM simulations reproduced fracture initiation, crack propagation, and global load-deflection patterns observed experimentally, especially for PW30%. However, deflections were underestimated due to simplified visco-plastic assumptions. Model refinements should include calibrated fracture energy, improved tensile softening descriptions, and incorporation of rate-dependent parameters to improve predictive accuracy.

PW30% is identified as the optimal replacement level, combining improved impact resistance and toughness with acceptable mechanical performance. It is most suitable for secondary or impact-prone elements such as protective barriers, crash-resistant panels, pavements, and industrial flooring. However, the reduction in compressive strength restricts its use in primary load-bearing members without further modification. This study was limited to a single type of PW, short-term mechanical testing, and no durability assessment. Future research should explore hybridization with fibers, surface modification of PW to enhance interfacial bonding, and durability studies under aggressive environments to expand the applicability of PW-modified concretes.

Acknowledgements

The authors express their sincere gratitude to the Ministry of Higher Education, Research and Innovation (MoHERI), Oman, for the financial support under grant reference MoHERI/BFP/ICEM/2022, which made this research possible.

References

1. Kalali, E.N., Lotfian, S., Shabestari, M.E., Khayatzadeh, S., Zhao, C., Nezhad, H.Y. (2023). A critical review of the current progress of plastic waste recycling technology in structural materials. Current Opinion in Green and Sustainable Chemistry, 40, 100763. https://doi.org/10.1016/j.cogsc.2023.100763.
2. Sau, D., Hazra, T., Shiuly, A. (2023). Microplastics in lentic environments: Implications for Indian ecosystems. Environmental Science and Pollution Research, 30(54), 114756-114778. https://doi.org/10.1007/s11356-023-30604-7.
3. Aldahdooh, M.A.A., Jamrah, A., Alnuaimi, A., Martini, M.I., Ahmed, M.S.R., Ahmed, A.S.R. (2018). Influence of various plastics-waste aggregates on properties of normal concrete. Journal of Building Engineering, 17, 13-22. https://doi.org/10.1016/j.jobe.2018.01.014.
4. Kurtoglu, A.E., Kaya, M., Eren, N.A. (2025). Modeling the strength of geopolymer concrete at high temperatures: Machine learning approach. Computers and Concrete, 35(6), 669-685. https://doi.org/10.12989/cac.2025.35.6.669.
5. Mazumder, E.A., Sapkota, S.C., Das, S., Saha, P., Samui, P. (2024). A generalized explainable approach to predict the hardened properties of self-compacting geopolymer concrete using machine learning techniques. Computers and Concrete, 34(3), 279-296. https://doi.org/10.12989/cac.2024.34.3.279.
6. Panda, S., Nanda, A., Panigrahi, S.K. (2024). Potential utilization of waste plastic in sustainable geopolymer concrete production: A review. Journal of Environmental Management, 366, 121705. https://doi.org/10.1016/j.jenvman.2024.121705.
7. Panda, S., Panigrahi, S.K. (2024). Production of sustainable GGBFS-based self-compacting geopolymer concrete containing E-waste aggregates under ambient temperature curing. Construction and Building Materials, 440, 137373. https://doi.org/10.1016/j.conbuildmat.2024.137373.
8. Panda, S., Panigrahi, S.K. (2025). Performance of waste rubber fiber and e-waste fiber in the realization of GGBFS-based self-compacting geopolymer concrete. Journal of Environmental Management, 393, 126999. https://doi.org/10.1016/j.jenvman.2025.126999.
9. Das, R., Nanda, A., Pradhan, J., Panigrahi, S.K. (2025). Realization of high-strength self-compacting geopolymer concrete through GGBFS-based ternary blended precursors and blended alkali-activated solution. European Journal of Environmental and Civil Engineering, 2025, 1-60. https://doi.org/10.1080/19648189.2025.2547297.
10. Panda, S., Pradhan, M., Panigrahi, S.K. (2025). Sustainable development of ternary binder-based mortar using OPC, GGBFS, and coal bottom ash. Construction and Building Materials, 496, 143862. https://doi.org/10.1016/j.conbuildmat.2025.143862.
11. Bhardwaj, B., Kumar, P. (2017). Waste foundry sand in concrete: A review. Construction and Building Materials, 156, 661-674. https://doi.org/10.1016/j.conbuildmat.2017.09.010.
12. Akçaözoğlu, S., Atiş, C.D., Akçaözoğlu, K. (2010). An investigation on the use of shredded waste PET bottles as aggregate in lightweight concrete. Waste management, 30(2), 285-290. https://doi.org/10.1016/j.wasman.2009.09.033.
13. Al-Tayeb, M.M., Daoor, I., Zeyad, A.M. (2020). Effect of partial replacements of coarse aggregate by polycarbonate plastic waste on the first crack impact resistance of concrete beam. Journal of Environment and Earth Science, 10(2), 55.
14. Mohammadhosseini, H., Tahir, M.M., Sam, A.R.M. (2018). RETRACTED: The feasibility of Improving impact resistance and strength properties of sustainable concrete composites by adding waste

metalized plastic fibres. Construction and Building Materials, 169, 223-236. https://doi.org/10.1016/j.conbuildmat.2018.02.210.
15. Mohammadhosseini, H., Tahir, M.M., Sam, A.R.M., Lim, N.H.A.S., Samadi, M. (2018). RETRACTED: Enhanced performance for aggressive environments of green concrete composites reinforced with waste carpet fibers and palm oil fuel ash. Journal of Cleaner Production, 185, 252. https://doi.org/10.1016/j.jclepro.2018.03.051.
16. Choi, Y.W., Moon, D.J., Chung, J.S., Cho, S.K. (2005). Effects of waste PET bottles aggregate on the properties of concrete. Cement and Concrete Research, 35(4), 776-781. https://doi.org/10.1016/j.cemconres.2004.05.014.
17. Marzouk, O.Y., Dheilly, R.M., Queneudec, M. (2007). Valorization of post-consumer waste plastic in cementitious concrete composites. Waste Management, 27(2), 310-318. https://doi.org/10.1016/j.wasman.2006.03.012.
18. Sobhan, K., Mashnad, M. (2002). Tensile strength and toughness of soil–cement–fly-ash composite reinforced with recycled high-density polyethylene strips. Journal of Materials in Civil Engineering, 14(2), 177-184. https://doi.org/10.1061/(ASCE)0899-1561(2002)14:2(177).
19. Al-Tayeb, M.M., Bakar, B.A., Ismail, H., Akil, H.M. (2012). Impact resistance of concrete with partial replacements of sand and cement by waste rubber. Polymer-Plastics Technology and Engineering, 51(12), 1230-1236. https://doi.org/10.1080/03602559.2012.696767.
20. Al-Tayeb, M.M., Bakar, B.H., Ismail, H., Akil, H.M. (2012). Experimental and nonlinear dynamic analysis of hybrid powder rubberized-normal concrete under impact load. Caspian Journal of Applied Sciences Research, 1(11), 23.
21. Al-Tayeb, M.M., Abu Bakar, B.H., Ismail, H., Akil, H.M. (2013). Impact energy for the first crack of reinforced concrete with partial replacements of sand by fine crumb rubber. Advanced Materials Research, 701, 286-290. https://doi.org/10.4028/www.scientific.net/AMR.701.286.
22. Abu Bakar, B.H., Al-Tayeb, M.M., Ismail, H., M. Akil, H. (2013). Impact energy for first crack of reinforced concrete with partial replacements of sand by rubber 1 mm particle size. Advanced Materials Research, 701, 261-264. https://doi.org/10.4028/www.scientific.net/AMR.701.261.
23. Al-Tayeb, M.M. (2017). Mechanical propagates of concrete with partial replacements of sand by plastic waste of vehicles under impact load. International Journal of Emerging Research in Management and Technology, 6(05), 19-25. https://doi.org/10.23956/ijermt/SV6N4/170.
24. Al-Tayeb, M.M., Ismail, H., Dawoud, O., Wafi, S.R., Al Daoor, I. (2017). Ultimate failure resistance of concrete with partial replacements of sand by waste plastic of vehicles under impact load. International Journal of Sustainable Built Environment, 6(2), 610-616. https://doi.org/10.1016/j.ijsbe.2017.12.008.
25. Al-Tayeb, M.M., Al Daoor, I., Wafi, S.R., Tayeh, B. (2020). Ultimate failure resistance of concrete with partial replacements of sand by polycarbonate plastic waste under impact load. Civil and Environmental Research, 12(2), 42.
26. Sau, D., Shiuly, A., Hazra, T. (2024). Utilization of plastic waste as replacement of natural aggregates in sustainable concrete: Effects on mechanical and durability properties. International Journal of Environmental Science and Technology, 21(2), 2085-2120. https://doi.org/10.1007/s13762-023-04946-1.
27. Nanda, A., Panda, S., Panigrahi, S.K. (2025). Production of durable conventional concrete using recycled HDPE and PET plastic coarse aggregate. Innovative Infrastructure Solutions, 10(3), 74. https://doi.org/10.1007/s41062-025-01886-2.
28. Vu, H.H., Do, T.G., Nguyen, T.T. (2020). The application of polypropylene fiber for reinforced concrete beams and slabs. IOP Conference Series: Materials Science and Engineering, 869(7), 072042. https://doi.org/10.1088/1757-899X/869/7/072042.
29. Kiyanets, A.V. (2018). Concrete with recycled polyethylene terephthalate fiber. Magazine of Civil Engineering, 8(84), 109-118. https://doi.org/10.18720/MCE.84.11.
30. Ismail, Z.Z., Al-Hashmi, E.A. (2008). Use of waste plastic in concrete mixture as aggregate replacement. Waste management, 28(11), 2041-2047. https://doi.org/10.1016/j.wasman.2007.08.023.
31. Naik, T.R., Singh, S.S., Huber, C.O., Brodersen, B.S. (1996). Use of post-consumer waste plastics in

cement-based composites. Cement and Concrete Research, 26(10), 1489-1492. https://doi.org/10.1016/0008-8846(96)00135-4.
32. Al-Manaseer, A.A., Dalal, T.R. (1997). Concrete containing plastic aggregates. Concrete International, 19(8), 47-52.
33. Sau, D., Shiuly, A., Hazra, T. (2023). Study on green concrete replacing natural fine and coarse aggregate by plastic waste-An experimental and machine learning approach. Materials Today: Proceedings, 2023, 1. https://doi.org/10.1016/j.matpr.2023.04.207.
34. Kim, S.B., Yi, N.H., Kim, H.Y., Kim, J.H.J., Song, Y.C. (2010). Material and structural performance evaluation of recycled PET fiber reinforced concrete. Cement and Concrete Composites, 32(3), 232-240. https://doi.org/10.1016/j.cemconcomp.2009.11.002.
35. Mwonga, M. M., Kabubo, C., Gathimba, N. (2023). Effect of polyethylene terephthalate fibres on the structural performance of reinforced concrete beams with openings in the shear region. Construction and Building Materials, 369, 130539. https://doi.org/10.1016/j.conbuildmat.2023.130539.
36. Aldahdooh, M.A. (2025). Multi-objective optimization of green concrete incorporating recycled plastic and sawdust waste as fine aggregates using response surface methodology. Structural Concrete, 26(3), 2951-2972. https://doi.org/10.1002/suco.70107.
37. Aldahdooh, M.A. (2025). RSM and hybrid machine learning for multi-objective optimization of sustainable concrete with plastic and sawdust wastes. ISRAA University Journal of Applied Science (IUJAS), 8(2), 1. https://doi.org/10.52865/yaqe2821.
38. Chao, Z., Wang, H., Hu, S., Wang, M., Xu, S., Zhang, W. (2024). Permeability and porosity of light-weight concrete with plastic waste aggregate: Experimental study and machine learning modelling. Construction and Building Materials, 411, 134465. https://doi.org/10.1016/j.conbuildmat.2023.134465.
39. Asif, U., Javed, M. F., Alyami, M., Hammad, A.W. (2024). Performance evaluation of concrete made with plastic waste using multi-expression programming. Materials Today Communications, 39, 108789. https://doi.org/10.1016/j.mtcomm.2024.108789.
40. Han, S.H., Khayat, K.H., Park, S., Yoon, J. (2024). Machine learning-based approach for optimizing mixture proportion of recycled plastic aggregate concrete considering compressive strength, dry density, and production cost. Journal of Building Engineering, 83, 108393. https://doi.org/10.1016/j.jobe.2023.108393.
41. Mandal, S., Shiuly, A., Sau, D., Mondal, A.K., Sarkar, K. (2024). Study on the use of different machine learning techniques for prediction of concrete properties from their mixture proportions with their deterministic and robust optimisation. AI in Civil Engineering, 3(1), 7. https://doi.org/10.1007/s43503-024-00024-8.
42. ACI 211.2-81 (1981). Standard practice for selecting proportions for structural lightweight concrete. American Concrete Institute, Farmington Hills, MI, USA.
43. Saikia, N., De Brito, J. (2012). Use of plastic waste as aggregate in cement mortar and concrete preparation: A review. Construction and Building Materials, 34, 385-401. https://doi.org/10.1016/j.conbuildmat.2012.02.066.
44. Asif, U., Javed, M.F., Abuhussain, M., Ali, M., Khan, W.A., Mohamed, A. (2024). Predicting the mechanical properties of plastic concrete: An optimization method by using genetic programming and ensemble learners. Case Studies in Construction Materials, 20, e03135. https://doi.org/10.1016/j.cscm.2024.e03135.
45. Asif, U., Javed, M.F., Alsekait, D.M., Aslam, F., Abd Elminaam, D.S. (2024). Data-driven evolutionary programming for evaluating the mechanical properties of concrete containing plastic waste. Case Studies in Construction Materials, 21, e03763. https://doi.org/10.1016/j.cscm.2024.e03763.
46. ASTM C31/C31M-06 (2006). Standard practice for making and curing concrete test specimens in the field. ASTM International, West Conshohocken, PA, USA.
47. Al-Tayeb, M.M., Abu Bakar, B.H., Akil, H.M., Ismail, H. (2013). Performance of rubberized and hybrid rubberized concrete structures under static and impact load conditions. Experimental Mechanics, 53(3), 377-384. https://doi.org/10.1007/s11340-012-9651-z.
48. Mustafa, M.A.T., Hanafi, I., Mahmoud, R., Tayeh, B.A. (2019). Effect of partial replacement of sand by

plastic waste on impact resistance of concrete: Experiment and simulation. Structures, 20, 519-526. https://doi.org/10.1016/j.istruc.2019.06.008.
49. Al-Tayeb, M.M., Abu Bakar, B.H., Ismail, H., Md Akil, H. (2013). Effect of partial replacement of sand by fine crumb rubber on impact load behavior of concrete beam: Experiment and nonlinear dynamic analysis. Materials and structures, 46(8), 1299-1307. https://doi.org/10.1617/s11527-012-9974-3.
50. Al-Tayeb, M.M., Zeyad, A.M., Dawoud, O., Tayeh, B.A. (2021). Experimental and numerical investigations of the influence of partial replacement of coarse aggregates by plastic waste on the impact load. International Journal of Sustainable Engineering, 14(4), 735-742. https://doi.org/10.1080/19397038.2020.1774820.
51. Al-Tayeb, M.M., Aisheh, Y.I.A., Qaidi, S.M., Tayeh, B.A. (2022). Experimental and simulation study on the impact resistance of concrete to replace high amounts of fine aggregate with plastic waste. Case Studies in Construction Materials, 17, e01324. https://doi.org/10.1016/j.cscm.2022.e01324.
52. Al-Tayeb, M.M., Bakar, B.A., Akil, H.M., Ismail, H. (2014). Experimental and numerical investigations of the influence of reducing cement by adding waste powder rubber on the impact behavior of concrete. Computers and Concrete, 11(1), 63-73. https://doi.org/10.12989/cac.2013.11.1.063.
53. Banthia, N.P. (1987). Impact resistance of concrete. Doctoral Dissertation, University of British Columbia, Vancouver, BC, Canada.
54. Banthia, N.P., Mindess, S., Bentur, A. (1987). Impact behaviour of concrete beams. Materials and Structures, 20(4), 293-302. https://doi.org/10.1007/BF02485926.
55. Banthia, N., Mindess, S., Bentur, A., Pigeon, M. (1989). Impact testing of concrete using a drop-weight impact machine. Experimental Mechanics, 29(1), 63-69. https://doi.org/10.1007/BF02327783.
56. Banthia, N., Gupta, P., Yan, C. (1999). Impact resistance of fiber reinforced wet-mix shotcrete part 1: Beam tests. Materials and Structures, 32(8), 563-570. https://doi.org/10.1007/BF02480490.
57. Oñate, E. (2009). Structural analysis with the finite element method: Linear statics. Springer Netherlands, Dordrecht, The Netherlands.
58. Al-Tayeb, M.M., Bakar, B.A., Ismail, H., Akil, H.M. (2013). Effect of partial replacement of sand by recycled fine crumb rubber on the performance of hybrid rubberized-normal concrete under impact load: Experiment and simulation. Journal of cleaner production, 59, 284-289. https://doi.org/10.1016/j.jclepro.2013.04.026.
59. Chopra, A.K. (2007). Dynamics of structures. Pearson Education India, Delhi, India.
60. Al-Tayeb, M.M., El-Daoor, I., Abu-Shaaban, N., Hamouda, H. (2015). Optimum superplasticizer added to rubberized concrete prepare by adding powder rubber as cement replacement. Journal of Multidisciplinary Engineering Science and Technology (JMEST), 2, 6.
61. Al-Tayeb, M., Abu-Shaaban, N., Al-Shorafa, M., Hamouda, H. (2015). Optimum superplasticizer added to concrete containing waste crumb rubber. Materials Science, Engineering, International Journal of Scientific and Technological Research, 2(6), 1.
62. Al-Tayeb, M.M., Hamouda, H. (2015). Effect of superplasticizer on workability of concrete containing crumb rubber. Civil and Environmental Research, 7(2), 35-43.
63. Asokan, P., Osmani, M., Price, A.D. (2010). Improvement of the mechanical properties of glass fibre reinforced plastic waste powder filled concrete. Construction and Building Materials, 24(4), 448-460. https://doi.org/10.1016/j.conbuildmat.2009.10.017.
64. Fu, H.C., Erki, M.A., Seckin, M. (1991). Review of effects of loading rate on concrete in compression. Journal of Structural Engineering, 117(12), 3645-3659. https://doi.org/10.1061/(ASCE)0733-9445(1991)117:12(3645).
65. Suaris, W., Shah, S.P. (1983). Properties of concrete subjected to impact. Journal of Structural Engineering, 109(7), 1727-1741. https://doi.org/10.1061/(ASCE)0733-9445(1983)109:7(1727).

Appendix

Table A1. Statistical analysis of raw data for PW0%, PW20%, PW30%, and PW40%

Mix ID	Test	Mean	SD	N (samples)
PW0%	Slump (mm)	165	7.5	3
PW20%		85	5.5	3
PW30%		55	4.2	3
PW40%		35	3.1	3
PW0%	Bulk density (kg/m^3)	2215	14.3	3
PW20%		1970	15.8	3
PW30%		1950	12.9	3
PW40%		1930	15.1	3
PW0%	CS (MPa)	43	0.8	3
PW20%		34	1.0	3
PW30%		28	1.1	3
PW40%		22	1.0	3
PW0%	MOE (GPa)	29.25	0.9	3
PW20%		24.14	0.9	3
PW30%		23.16	1.0	3
PW40%		20.84	1..1	3
PW0%	Peak bending load (N)	8080	183	6
PW20%		12910	245	6
PW30%		13710	222	6
PW40%		9270	217	6
PW0%	GF (Nm, dynamic)	1.43	0.2	6
PW20%		2.42	0.4	6
PW30%		3.62	0.3	6
PW40%		3.25	0.3	6